Hydrol. Earth Syst. Sci. Discuss., 6, 2075–2098, 2009
www.hydrol-earth-syst-sci-discuss.net/6/2075/2009/

Hydrology and Earth System Sciences Discussions

Papers published in *Hydrology and Earth System Sciences Discussions* are under open-access review for the journal *Hydrology and Earth System Sciences*

Deriving inherent optical properties and associated uncertainties for the Dutch inland waters during the Eagle Campaign

M. S. Salama[1], **Z. Su**[1], **C. M. Mannaerts**[1], **and W. Verhoef**[1,2]

[1]International Institute for Geo-Information Science and Earth Observation, Enschede, The Netherlands
[2]The National Aerospace Laboratory NLR, Emmeloord, The Netherlands

Received: 13 February 2009 – Accepted: 24 February 2009 – Published: 9 March 2009

Correspondence to: M. S. Salama (salama@itc.nl)

Published by Copernicus Publications on behalf of the European Geosciences Union.

Abstract

During the Eagle 2006 campaign intensive in-situ and air/space borne measurements were carried out over the Wolderwijd and Veluwemeer natural waters in the Netherlands. In this paper, we modify the GSM semi-analytical inversion model for these lakes to derive inherent optical properties (IOPs) and their spectral dependencies from air and space borne data. Uncertainties of the derived IOPs are estimated using a nonlinear regression technique. The modified model succeeded in deriving accurate estimates of IOPs with R^2 higher than 0.9 and RMSE values equal to 0.12 and 0.05 for absorption and scattering coefficients, respectively. Finally, we show that the uncertainty of derived absorption coefficients is slightly independent of absorption's magnitude. While the uncertainty of all derived IOPs increases with water turbidity.

1 Introduction

Lakes are important natural water resources yet they are seriously threatened by eutrophication, salinisation and heavy metal contamination. Increased sediment loads paly an important role in water quality of lakes since they relate total primary production to heavy metal and micro pollutants (Vos et al., 1998). Traditional measurements of water quality are costly, time-consuming and are limited in their spatial and temporal coverage. Remote sensing data facilitate acquiring synoptic information of water quality at high temporal frequency. Monitoring of water quality using remote sensing, in conjunction with strategic in-situ sampling can play a crucial role in determining the current status of water quality conditions and helps anticipate, mitigate and even avoid future water catastrophes (GEOSS, 2007). Remote sensing of inland waters is quite challenging due to the complicated signals from turbid water, bottom reflectance and adjacent land surfaces. Moreover the empirical nature of the retrieval algorithms limits their application to a specific range of concentrations, area and season. Kallio et al. (2001) studied different algorithms to estimate chlorophyll-*a* in lakes. These algorithms

were empirical and estimated one variable using band-ratio of approximately 675 nm and 705 nm (Dekker et al., 1992; Gitelson et al., 1993). A generalized retrieval algorithm is, however, hindered by the large natural variability of inland waters. Significant efforts on improving the accuracy of air and space borne derived water quality parameters are therefore required for inland and near coastal waters. Many studies have used semi analytical models to derive water quality parameters in lakes (Hoogenboom et al., 1998; Gons et al., 2002). Derived water quality parameters from multi variable inversion methods are ambiguous and not unique (Sydor et al., 2004). Our knowledge on the uncertainty of derived IOPs is, therefore, as important as the values of the estimates. The ambiguity resulting from noise and atmospheric correction could partially be captured by a reliable measure of uncertainty (Salama, 2003). In general, nonlinear regression techniques (Bates and Watts, 1988) are employed to derive the uncertainty of estimates from ocean color data (Salama, 2003; Wang et al., 2005; Maritorena and Siegel, 2005). Other promising methods are used when the inversion employs look up tables (Van der Woerd and Pasterkamp, 2008). In this paper we modify the GSM semi-analytical inversion model to derive inherent optical properties (IOPs) and their spectral dependencies. The total uncertainties of the derived products are then estimated using a nonlinear regression technique.

2 Method

The total remote sensing reflectance received at the sensor level can be written as the sum of several components (Gordon, 1997):

$$Rs_t(\lambda) = Rs_r(\lambda) + Rs_a(\lambda) + T_v(\lambda)\{Rs_{sfc}(\lambda) + Rs_w(\lambda)\} \quad (1)$$

where $T_v(\lambda)$ is the viewing diffuse transmittance from the water surface to the sensor. The subscript of the reflectance represents the contribution from air molecules *r*, aerosol *a*, surface *sfc*, and water *w*. The calculation of Rayleigh scattering of air molecules is well described in terms of geometry and pressure (Gordon et al., 1988a).

Water surface reflectance can be estimated using statistical relationships and wind speed (Cox and Munk, 1954a,b). Gaseous transmittance can be calculated from ancillary data on ozone and water vapor content using transmittance models (Goody, 1964; Malkmus, 1967). Viewing diffuse transmittance is approximated following Gordon et al. (1983). Aerosol scattering can be evaluated from measured aerosol optical thickness and assumed aerosol type. This information about the atmospheric path reflectance facilitates the retrieval of the signal leaving the water body i.e. Rs_w. Water remote sensing reflectance $Rs_w(\lambda)$ can be related to the inherent optical properties (IOPs) of the water column as (GSM model: Maritorena et al., 2002):

$$Rs_w(\lambda) = \frac{t}{n_w^2} \sum_{i=1}^{2} g_i \left(\frac{b_b(\lambda)}{b_b(\lambda) + a(\lambda)} \right)^i \quad (2)$$

where g_1, g_2 are subsurface expansion coefficients due to internal refraction, reflection and sun zenith; t and n_w are the sea air transmission and water index of refraction, respectively. Their values are taken from literature (Gordon et al., 1988b; Maritorena et al., 2002; Lee, 2006). The parameters $b_b(\lambda)$ and $a(\lambda)$ are the bulk backscattering and absorption coefficients of the water column. Case II water is considered with three independently varying constituents, namely: chlorophyll-*a* (Chl-*a*), detritus and dissolved organic matter (dg) and suspended particulate matter (SPM). The absorption and backscattering coefficients are modeled as being the sum of absorption and backscattering from all water constituents:

$$a(\lambda) = a_w(\lambda) + a_p(\lambda) + a_{dg}(\lambda) \quad (3)$$

$$b_b(\lambda) = 0.5 b_w(\lambda) + \alpha b_{\text{spm}}(\lambda) \quad (4)$$

The absorption and scattering coefficients of water molecules, a_w and b_w, were assumed constants. Their values were obtained from (Pop and Fry, 1997; Mobley, 1994), respectively.

The total absorption of phytoplankton pigments a_p is approximated as (Lee et al., 1999):

$$a_p(\lambda) = a_0(\lambda)a_p(0.44) + a_1(\lambda)a_p(0.44)\ln a_p(0.44) \quad (5)$$

where $a_0(\lambda)$ and $a_1(\lambda)$ are empirical coefficients. The absorption effects of detritus and dissolved organic matter are combined due to the similar spectral signature (Maritorena et al., 2002) and approximated using the model (Bricaud et al., 1981):

$$a_{dg}(\lambda) = a_{dg}(440)\exp[-s(\lambda - 440)] \quad (6)$$

where s is an unknown spectral exponent. The scattering coefficient of SPM b_{spm} is parameterized as (Kopelevich, 1983):

$$b_{spm}(\lambda) = b_{spm}(550)\left(\frac{550}{\lambda}\right)^{y} \quad (7)$$

where y is the unknown spectral shape parameter. The backscattering fraction α is estimated from the "San Diego harbor" scattering phase function (Petzold, 1977).

Five parameters are derived by inverting Eq. (2) using nonlinear optimization (Lee et al., 1999; Maritorena et al., 2002). These parameters are called the set of IOPs and denoted as a vector **iop**:

$$\mathbf{iop} = \begin{bmatrix} a_p(440) \\ a_{dg}(440) \\ b_{spm}(550) \\ s \\ y \end{bmatrix} \quad (8)$$

In this work we assume the absorption and back/scattering coefficients of any constituent to be linearly related to its concentration and specific inherent optical property (SIOPs). SIOP values of the Dutch lakes are obtained from the measurements of Hakvoort et al. (2002).

We refer to both parameters, concentration and absorption/(back)scattering coefficients, using the same abbreviation of the constituent itself i.e., dg, Chl-*a*, SPM.

3 Study area and data set

Field measurements of water leaving reflectance, turbidity and chlorophyll-*a* of the Wolderwijd and Veluwemeer (52°19′12.0″N, 05°36′12.0″E) natural waters were carried out at eight sites during the Eagle 2006 campaign. Table 1 shows the locations of these sites and measured concatenations of SPM and Chl-*a* in the lab. Measured spectra of water leaving reflectance are shown in Fig. 1.

This limited number of truth data encumbers the validation of model performance. Therefore, radiative transfer simulations, at 30° sun zenith, of a synesthetic set of IOPs (Lee, 2006, IOCCG data set) were used in combination with field measured spectra and IOPs. The IOPs of each sampling site are computed from measured concentrations and published values of specific inherent optical properties for the Dutch lakes (Hakvoort et al., 2002). IOPs and SIOPs were assumed to be linearly related, i.e. the IOP of a constituent is equal to its concentration times its SIOPs (Bricaud et al., 1995). The field campaign was also associated with hyperspectral airborne measurements from the Airborne Hyperspectral Spectrometer (AHS) (Fernández-Renau et al., 2005). MEdium Resolution Imaging Spectrometer (MERIS) and Advanced Space borne Thermal Emission and Reflection Radiometer (ASTER) observations were also available during the Eagle 2006 campaign. Table 2 summarizes the used data sets in this work. For more details on data availabilities and specifications, the reader is encouraged to consult the Eagle 2006 data acquisition reports (Timmermans et al., 2007; Su et al., 2009).

4 Results

4.1 Model performance

Measured spectra and IOPs are combined with IOCCG data set to form the validation set for this study.

For MERIS, AHS and the validation data sets, the inversion of the GSM model is adapted to derive five parameters in visible bands covering the wavelengths from 400 nm to 850 nm. The Levenberg-Marquardt Algorithm (LMA) is employed using a constrained nonlinear optimization (Press et al., 2002). The constraints are set such that they guarantee positive values of retrieved IOPs. The performance of the adapted GSM inversion model is tested using IOCCG and measured data sets. Model derived IOPs are compared to the known values, synthesized plus measured, in Fig. 2. Four IOPs are shown: three absorption coefficients $a_p(440)$, $a_{dg}(440)$, $a_{\text{total}}(440)$ and one scattering coefficient $b_{\text{spm}}(550)$.

The root mean square of error RMSE, R^2 and the statistical parameters of model II regression (Laws, 1997) for log-transformed data are used to evaluate the performance of inversion as shown in Table 3.

The derived IOPs are within acceptable accuracy, i.e. the R^2 is higher than 0.9 for the four derived IOPs. The derived scattering coefficient at 550 nm has the highest accuracy with RMSE value less than 0.06 and $R^2 \sim 0.98$. The uncertainties in the retrieved absorption coefficients are large, particularly the value of $a_p(440)$ with a RMSE value ~1.15.

4.2 Intercomparison of remotely sensed products

Available images are geo-referenced and converted to at-sensor-reflectance. Atmospheric path correction is then preformed using the radiative transfer method of Vermote et al. (1997). Gaseous transmittances of ozone, oxygen, carbon dioxide, methane and nitrous oxide are assumed constant over the study region. Measured values of aerosol optical thickness during the the Eagle 2006 campaign are used to run the computation, assuming an urban aerosol. The adjacency effects from the surrounding lands was accounted for in the computation. The IOPs are derived using the constrained LMA. This method is applied on MERIS and AHS spectra, while another method is used for ASTER image. The spectral characteristics of ASTER constrain the

application of such nonlinear fit method. Instead, matrix inversion method (Hoge and Lyon, 1996) is applied on ASTER's two visible bands assuming $a_{dg}(440)=0.25\,m^{-1}$. In consequence only two variables were retrieved from ASTER image, namely SPM scattering and Chl-*a* absorption coefficients. An intercomparison between retrieved values of SPM scattering and Chl-*a* and dg absorptions are shown in Fig. 3 for two cross sections over the Veluwemeer (start 52.38307, 5.63710, end 52.3681, 5.65516) and the Wolderwijd (start 52.34515, 5.60731, end 52.3579, 5.59198). There is a very good match between the products of AHS and MERIS while retrieved values from ASTER are patchy and don't correspond to derived IOPs from other sensors.

4.3 Uncertainties of AHS derived IOPs

The nonlinear regression method of Bates and Watts (1988) is used to estimate the uncertainties of derived IOPs. However, this approach is only applicable with nonlinear optimization techniques. We used nonlinear optimization with AHS and MERIS but not with ASTER. To derive the uncertainty of ASTER products, another method is needed (Salama and Stein, 2009). However we will limit the discussion to the uncertainty maps associated with AHS products. We will use the standard deviation (STD) at 95% of confidence as quantitative measure of uncertainty. The uncertainties of AHS derived IOPs are shown in Fig. 4. The uncertainty maps of IOPs have similar spatial variations and their values increase proportionally to water turbidity as shown in Fig. 5.

5 Discussion

5.1 Inversion

The modified GSM succeeded in deriving the IOPs with R^2 higher than 0.9 and 100% of valid retrievals, we refer to (Lee, 2006, pp. 83–84) for comparison. However the RMSE values of the retrieved absorption coefficients are large, particularly for Chl-*a*.

These large errors can be attributed to three main reasons; (i) GSM model can greatly overestimate chlorophyll-*a* in turbid waters (D'Sa and Miller, 2005); (ii) the parametrization in Eq. (5) ignores the great variability of Chl-*a* absorption as measured in nature (Bricaud et al., 1995, 1998; Carder et al., 1999); (iii) the overlapped absorption spectra of dg and Chl-*a* at 440 nm will encumber their retrieval. In other words, the retrievals of dg absorption coefficient tend to slightly underestimate known values at low end and slightly overestimate at the high end. This trend is inverted for the derived values of Chl-*a* absorption coefficient. These effects of over/under estimations will compensate each other when the total absorption coefficient is evaluated. This can be observed by the increased accuracy of derived total absorption with RMSE value of 0.12 and R^2~0.97. The highest accuracy was obtained for the derived SPM scattering coefficient at 550 nm with RMSE value less than 0.06 and R^2=0.98. The high accuracy of derived SPM scattering coefficient is due to including the red and Near Infra Red (NIR) bands in the inversion. At this part of the spectrum, water absorption and SPM backscattering are the major contributors to the observed reflectance. For example, at wavelength 780 nm the water absorption is invariant to water temperature (Hakvoort, 1994) and thus the reflectance will linearly respond to any increase in SPM concentration. This linearity between reflectance and SPM backscattering at the red and NIR region will stabilize the inversion and reduce the uncertainty.

5.2 Remotely sensed products

The derived values of SPM scattering and Chl-*a* absorption from ASTER are patchy and did not reflect the spatial variability as observed from MERIS and AHS. This can be attributed to the retrieval method applied on ASTER. The inversion of ASTER was based on matrix inversion of Eq. (2) in two bands with a constant value of dg absorption coefficient at 440 nm (=0.25 m^{-1}). On the other hand, the retrieval method of MERIS and AHS was based on nonlinear optimization for five variables in all visible bands i.e. 15 for MERIS and 16 for AHS. There is a very good match in the retrieved values of SPM scattering at the Veluwemeer (Fig. 3e) and Chl-*a* absorptions at the Wolderwijd

(Fig. 3b). However, slight overestimation of Chl-*a* absorption and underestimation of SPM scattering coefficients with-respect-to (w.r.t.) AHS can be observed in Fig. 3a and Fig. 3f respectively. The values of dg absorption coefficient are generally overestimated w.r.t. AHS retrieved values, with the same spatial variation, however. The differences between MERIS and AHS results may be attributed to imperfect atmospheric correction and inappropriate spectral coverage of AHS for Chl-*a* retrieval. On the one hand, the longer atmospheric path of MERIS w.r.t. AHS signals increases the contributions of aerosol scattering and illumination-viewing variations to the top of atmosphere (TOA) reflectance. It is also noted that AHS spectral range does not cover chlorophyll-*a* absorption feature centered at 440 nm. This absorption feature is of quite importance for reliable estimation of Chl-*a* and dg absorption coefficients. The combined effects of the longer atmospheric path and the absence of 440 nm absorption feature will increases the uncertainties on the retrieved values of dg and Chl-*a*. A major limitation in this work is that air and space borne images were not concurrent with field measurements such that independent validation of remotely sensed products was not possible.

5.3 Uncertainties

The method of Bates and Watts (1988) was used to estimate the uncertainties of derived IOPs. However, this approach is adequate as long as model inversion has a well conditioned Jacobian matrix of the minimum cost function. It reflects how well the model can fit the observation but not how well the derived parameters fit the measured values. The estimated uncertainties (Fig. 4), therefore do not reflect the actual uncertainties which are presented in Table 3 as RMSE values. This total uncertainty of derived values can roughly be assigned to three main causes: residuals, numerical and physical sources. Residuals are errors originated from sensor noise and imperfect atmospheric correction or any other correction. The numerical part is related to the used numeric technique in the inversion. The physical uncertainty is caused by two distinctive sources: bio-optical model approximations and the intrinsic relation between apparent and inherent optical properties of the water column which causes reflectance

ambiguity. The later is an inherent problem to remote sensing of water quality (Sydor et al., 2004). In this sense, mainly model approximation and inversion accuracy were quantified in Fig. 4. To quantify all sources of error, newly emerging methods are promising (Salama and Stein, 2009). Figure 4 shows that there are weak relationships between derived values of absorption coefficients and associated uncertainties. This is not the case for the scattering where a clear relationship can be observed (Fig. 4c). The error increases exponentially with the magnitude of derived values. Actually, the uncertainty of all IOPs increase proportionally to water turbidity (Fig. 5). Therefore, larger errors are expected in turbid waters. Two water types can be distinguished from the right panels of Fig. 4 and Fig. 5. The pixels within the gray region have STD values less than the value of the corresponding IOPs. These pixels correspond to relatively smaller range of derived IOPs. The remaining pixels, which form the majority, have their STD values higher than the retrieved values of IOPs, i.e. uncertainty is more than 100%. More investigation and measurements are required to understand the reason of this grouping. This kind of comparison between derived values and their uncertainties has been found useful for resolving the sub-pixel variability of earth observation hydrological products (Van der Velde et al., 2008).

6 Conclusions

In this paper the GSM model was modified to retrieve five parameters: three IOPs and two spectral exponents. The method is applied on MERIS and AHS and validated using measured and IOCCG data sets. Due to the limited number of field measurements, 8 only, measured data were combined with the IOCCG data set to form validation set. Some preliminary conclusions can be drawn from the results of this work:

– The adapted inversion method derived accurate estimates of all IOPs with R^2 values higher than 0.9 and RMSE values equal to 0.12 and 0.05 for absorption and scattering coefficients, respectively.

- ASTER's derived IOPs are very patchy and their values are generally higher than those retrieved from MERIS and AHS. Except for dg, there was a very good match between MERIS and AHS products.

- The uncertainty of derived absorption coefficients is slightly independent of absorption magnitude. While the uncertainty of all derived IOPs increased with water turbidity.

- Uncertainty maps are simultaneously estimated for each retrieved IOP. This information forms a benchmark for validation and fusion of remote sensing products of water quality parameters. This technique can be used to validate earth observation products of water quality in remote areas where few or no in-situ measurements are available.

Acknowledgements. The authors would like to thank the European Space Agency (ESA) for supporting this research and supplying MERIS data, the Instituto Nacional de Técnica Aeroespacial (INTA) for providing high quality hyperspectral dataset and technical assistance, the National Aeronautics and Space Administration (NASA) for providing ASTER data, the Eagle 2006 team for collecting and archiving in-situ measurements. The financial support of ESA, arrangement No. 20239/06/I-LG, is gratefully acknowledged.

References

Bates, D. and Watts, D.: Nonlinear Regression Analysis and Its Applications, John Wiley and Sons, NY, 365 pp., 1988. 2077, 2082, 2084

Bricaud, A., Morel, A., and Prieur, L.: Absorption by dissolved organic-matter of the sea (yellow substance) in the UV and visible domains, Limnol. Oceanogr., 26, 43–53, 1981. 2079

Bricaud, A., Babin, M., Morel, A., and Claustre, H.: Variability in the chlorophyll-specific absorption coefficients of naturnal phytoplankton: Analysis and parameterization, J. Geophys. Res., 100, 13321–13332, 1995. 2080, 2083

Bricaud, A., Morel, A., Babin, M., Allali, K., and Claustre, H.: Variations of light absorption by suspended particles with chlorophyll a concentration in oceanic (case 1) waters: Analysis and implications for bio-optical models, J. Geophys. Res., 103, 1998. 2083

Carder, K., Chen, F., Lee, Z., Hawes, S., and Kamykowski, D.: Semianalytical Moderate-Resolution Imaging Spectrometer algorithms for chlorophyll-*a* and absorption with bio-optical domains based on nitrate-depletion temperature, J. Geophys. Res., 104, 5403–5421, 1999. 2083

Cox, C. and Munk, W.: Measurements of the roughness of the sea surface from photographs of the sun glitter, J. Opt. Soc. Am., 44, 838–850, 1954a. 2078

Cox, C. and Munk, W.: Statistics of the sea surface derived from sun glitter, J. Mar. Res., 13, 198–227, 1954b. 2078

Dekker, A., Malthus, T., Wijnen, M., and Seyhan, E.: Remote sensing as a tool for assessing water quality in Loosdrecht Lakes, Hydrobiologia, 233, 137–159, 1992. 2077

D'Sa, E. and Miller, R.: Bio-optical properties of coastal waters., in: Remote Sensing of Coastal Aquatic Environments, edited by Miller, R., del Castillo, C., and McKee, B., 129–155, Springer, Dordrecht, The Netherlands, 2005. 2083

Fernández-Renau, A., Gómez, J. A., and De Miguel, E.: The INTA-AHS system. in: SPIE proceeding of Sensors, Systems and Next-Generation Satellites IX, vol. 5978, 471–478, 2005. 2080

GEOSS: GEO Inland and Nearshore Coastal Water Quality Remote Sensing, in: GEO group on earth observation, edited by: Bauer, M., Dekker, A., DiGiacomo, P., Greb, S., Gitelson, A., Herlevi, A., and Kutser, T., GEO, 2007. 2076

Gitelson, A., Garbuzov, G., Szilagyi, F., Mittenzwey, K. H., Karnieli, A., and Kaiser, A.: Quantitative remote sensing methods for real-time monitoring of inland waters quality, Int. J. Remote Sens., 14, 1269–1295, 1993. 2077

Gons, H., Rijkeboer, M., and Ruddick, K.: A chlorophyll-retrieval algorithm for satellite imagery (Medium Resolution Imaging Spectrometer) of inland and coastal waters, J. Plankton Res., 24, 947–951, 2002. 2077

Goody, R.: Atmospheric radiation 1, theoretical basis, Oxford University Press, 544 pp., 1964. 2078

Gordon, H.: Atmospheric correction of ocean color imagery in the Earth Observing System era, J. Geophys. Res., 102, 17081–17106, 1997. 2077

Gordon, H., Clark, D., Brown, J., Brown, O., Evans, R., and Broenkow, W.: Phytoplankton

pigment concentrations in the middle Atlantic bight: comparison of ship determinations and CZCS estimates, Appl. Optics, 22, 20–36, 1983. 2078

Gordon, H., Brown, J., and Evans, R.: Exact Rayleigh scattering calculation for the use with the Nimbus-7 Coastal Zone Color Scanner, Appl. Optics, 27, 862–871, 1988a. 2077

Gordon, H., Brown, O., Evans, R., Brown, J., Smith, R., Baker, K., and Clark, D.: A semianalytical radiance model of ocean color, J. Geophys. Res., 10909–10924, 1988b. 2078

Hakvoort, H.: Absorption of light by surface water, Ph.d., Technische Universiteit Delft, 1994. 2083

Hakvoort, H., de Haan, J., Jordans, R., Vos, R., Peters, S., and Rijkeboer, M.: Towards airborne remote sensing of water quality in The Netherlands–validation and error analysis, ISPRS Journal of Photogrammetry and Remote Sensing, 57, 171–183, 2002. 2079, 2080

Hoge, F. E. and Lyon, P. E.: Satellite retrieval of inherent optical properties by linear matrix inversion of ocean radiance models: An analysis of model and radiance measurement errors, J. Geophys. Res., 101, 16631–16648, 1996. 2082

Hoogenboom, H., Dekker, A., and De Haan, J.: Retrieval of chlorophyll a and suspended matter in inland waters from Casi data by matrix inversion, Can. J. Remote Sens., 24, 144–152, 1998. 2077

Kallio, K., Kutser, T., Hannonen, T., Koponen, S., Pulliainen, J., Vepsalainen, J., and Pyhalahti, T.: Retrieval of water quality from airborne imaging spectrometry of various lake types in different seasons, Sci. Total Environ., 208, 59–77, 2001. 2076

Kopelevich, O.: Small-parameter model of optical properties of sea waters, vol.1, Physical Ocean Optics, Nauka, 1983. 2079

Laws, E.: Mathematical Methods for Oceanographers: An introduction, John Wiley and Sons, New York, 343 pp., 1997. 2081

Lee, Z.: Remote Sensing of Inherent Optical Properties: Fundamentals, Tests of Algorithms, and Applications, Tech. Rep. 5, International Ocean-Colour Coordinating Group, 2006. 2078, 2080, 2082

Lee, Z., Carder, K., Mobley, C., Steward, R., and Patch, J.: Hyperspectral remote sensing for shallow waters: 2. Deriving bottom depths and water properties by optimization, Appl. Optics, 38, 3831–3843, 1999. 2079

Malkmus, W.: Random Lorentz band model with exponential-tailed S-1 line intensity distribution function, J. Opt. Soc. Am., 57, 323–329, 1967. 2078

Maritorena, S. and Siegel, D.: Consistent merging of satellite ocean color data sets using a

bio-optical model, Remote Sens. Environ., 94, 429–440, 2005. 2077
Maritorena, S., Siegel, D., and Peterson, A.: Optimization of a semianalytical ocean color model for global-scale applications, Appl. Optics, 41, 2705–2714, 2002. 2078, 2079
Mobley, C.: Light and water radiative transfer in natural waters, Academic Press, 592 pp., 1994. 2078
Petzold, T.: Volume scattering functions for selected ocean waters, in: Light in the Sea, edited by: Tyler, J., vol. 12, pp. 150–174, Dowden, Hutchinson and Ross, Stroudsburg, Pa. USA, 1977. 2079
Pop, R. and Fry, E.: Absorption spectrum (380-700nm) of pure water: II, Integrating cavity measurements, Appl. Optics, 36, 8710–8723, 1997. 2078
Press, W., Teukolsky, S., Vetterling, W., and Flannery, B.: Numerical recipes in C++, The art of scientific computing, Cambridge University Press, 1002 pp., 2002. 2081
Salama, M. and Stein, A.: Error decomposition and estimation of inherent optical properties, in review, Appl. Optics, 2009. 2082, 2085
Salama, M. S.: Optical remote sensing for the estimation of marine bio-geophysical quantities, Ph.d., Katholieke Universiteit Leuven, 2003. 2077
Su, Z., Timmermans, W., Van der Tol, C., Dost, R., Bianchi, R., Gmez, J., House, A., Hajnsek, I., Menenti, M., Magliulo, V., Esposito, M., Haarbrink, R., Bosveld, F., Rothe, R., Baltink, H., Vekerdy, Z., Sobrino, J., Timmermans, J., van Laake, P., Salama, M. S., Van der Kwast, H., Claassen, E., Stolk, A., Jia, L., Moors, E., O., H., and Gillespie, A.: EAGLE 2006 Multi-purpose, multi-angle and multi-sensor in-situ and airborne campaigns over grassland and forest, Hydrol. Earth Syst. Sci. Discuss., in press, 2009. 2080
Sydor, M., Gould, R., Arnone, R., Haltrin, V., and Goode, W.: Uniqueness in Remote Sensing of the Inherent Optical Properties of Ocean Water, Appl. Optics, 43, 2156–2162, 2004. 2077, 2085
Timmermans, W., Dost, R., and Su, Z.: EAGLE 2006 EAGLE Netherlands multi-purpose, multi-angle and multi-sensor in-situ, airborne and spaceborne campaigns over grassland and forest, Tech. rep., Department of Water Resources International Institute for Geo-Information Science and Earth Observation, ITC, 2007. 2080
Van der Velde, R., Su, Z., and Ma, Y.: Impact of soil moisture dynamics on ASAR so signatures and its spatial variability observed over the Tibetan Plateau, Sensors, 8, 5479–5491, 2008. 2085
Van der Woerd, H. and Pasterkamp, R.: HYDROPT: A fast and flexible method to retrieve

chlorophyll-*a* from multispectral satellite observations of optically complex coastal waters, Remote Sens. Environ., 112, 1795–1807, 2008. 2077

Vermote, E., Tanre, D., Deuze, J., Herman, M., and Morcrette, J.: Second simulation of the satellite signal in the solar spectrum, 6S: An overview, IEEE T. Geosci. Remote, 35, 675–686, 1997. 2081

Vos, R., Villars, M., Roozekrans, J., Peters, S., and Raaphorst, W. V.: Integrated monitoring of total suspended sediment in the Dutch coastal zone, Tech. rep., part II, 1998. 2076

Wang, P., Boss, E., and Roesler, C.: Uncertainties of inherent optical properties obtained from semianalytical inversions of ocean color, Appl. Optics, 44, 4074–4084, 2005. 2077

Table 1. Locations of the sampling sites and measured concentrations.

site	Lat	Long	SPM mg/l	Chl-$a\mu$g/l
P1	52.37481	5.63524	5.8	10
P2	52.38326	5.63874	4.5	7
P3	52.37735	5.65598	1.9	2
P4	52.37566	5.66849	3.0	6
P5	52.39295	5.65845	2.8	9
P6	52.38732	5.64361	3.9	6
P7	52.37570	5.62356	3.4	7
P8	52.36788	5.63584	0.9	4

Table 2. Summary of the subset from Eagle2006 dataset used in this study.

Acquisition	Sensor	Description	Date
Space borne	MERIS	FR level L1b	08-06-2006
Space borne	ASTER	level L1b	08-06-2006
Airborne	AHS	Level L1b	13-06-2006
Field measurements	ASD	raw spectra	04-07-2006
Field measurements		water samples	04-07-2006
IOCCG	synthesized	spectra and IOPs	

Table 3. RMSE and regression (type II) results for the IOCCG (500 values) and measured data set (8 values) at 440 nm and 550 nm.

iops	n	Intercept	slope	R^2	RMSE
$a_p(440)$	508	0.0039	0.92	0.91	1.145
$a_{dg}(440)$	500	0.0097	1.35	0.94	0.212
$a(440)$	500	−0.0041	1.27	0.97	0.122
$b_{spm}(550)$	508	−0.0515	1.02	0.98	0.05

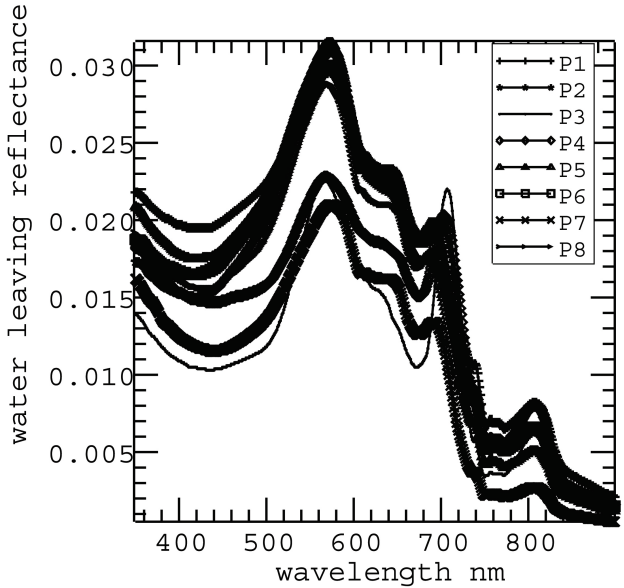

Fig. 1. Measured water leaving reflectance in 8 sites.

HESSD
6, 2075–2098, 2009

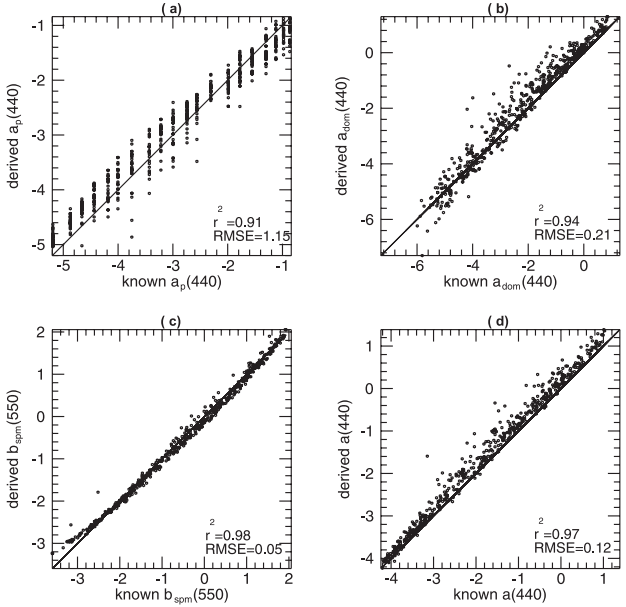

Fig. 2. Comparison between the derived and known values using IOCCG and measured data for **(a)**: chlorophyll-*a* absorption coefficient at 440 nm, **(b)**: dg absorption coefficient at 440 nm, **(c)**: SPM scattering coefficient at 550 nm and **(d)**: total absorption coefficient at 440 nm.

HESSD
6, 2075–2098, 2009

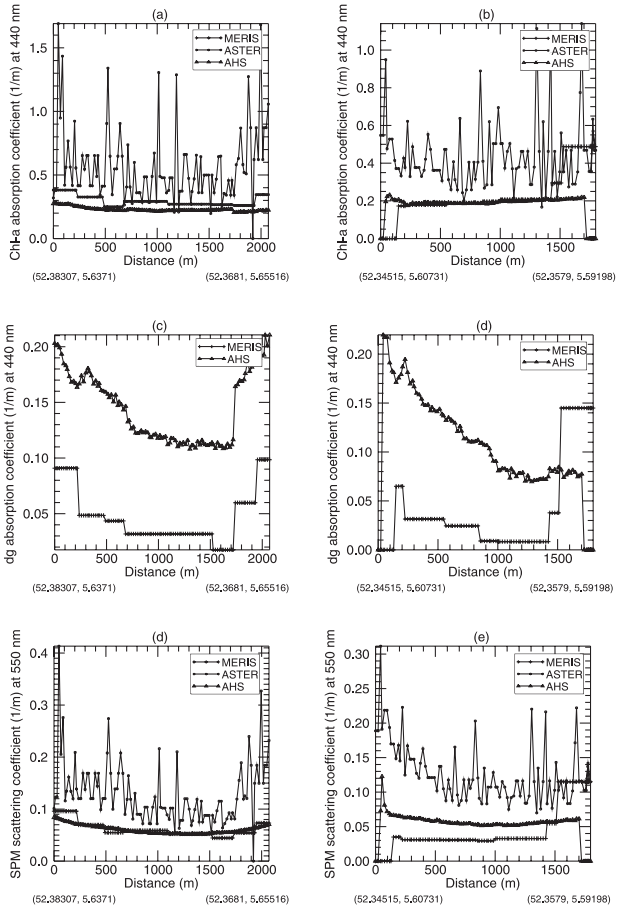

Fig. 3. Intercomparison of IOPs derived from different sensors for a cross-section at the Veluwemeer (Fig. **a, c, e**) and a cross-section at the Wolderwijd (Fig. **b, d, f**). The derived IOPs are: Chl-*a* (a and b), dg (c and d) and SPM (e and f).

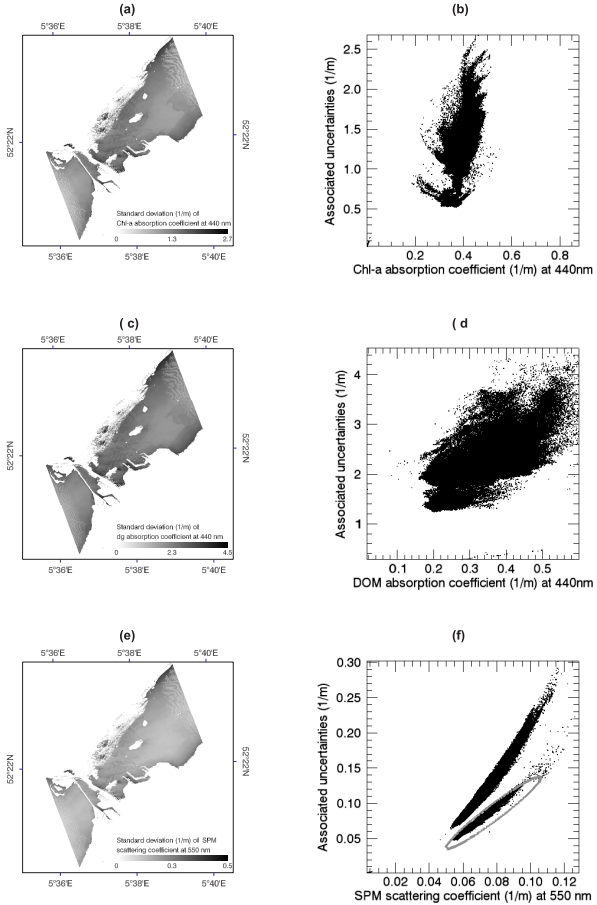

Fig. 4. The standard deviation (STD) maps for each of the retrieved IOPs from AHS data set of **(a)**: Chl-*a* , **(c)**: dg and **(e)**: SPM. Right panels (Fig. **b, d, f**) illustrate the scatter plot between standard deviations values on the Y-axis and the corresponding IOPs values on the X-axis.

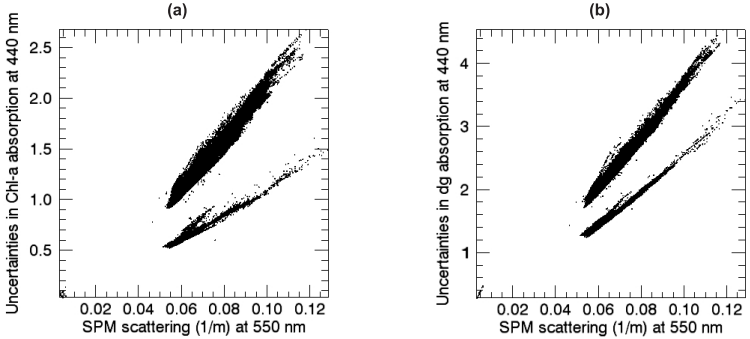

Fig. 5. The standard deviation (STD) of derived: **(a)** Chl-*a* and **(b)** dg absorption coefficients as function of the estimated values of SPM scattering.